forests

MDPI

Article

August Temperature Reconstruction Based on Tree-Ring Latewood Blue Intensity in the Southeastern Tibetan Plateau

Teng Li [1] and Jinbao Li [2,3,*]

[1] School of Geography and Remote Sensing, Guangzhou University, Guangzhou 510006, China; liteng@gzhu.edu.cn
[2] Department of Geography, University of Hong Kong, Hong Kong SAR 999077, China
[3] HKU Shenzhen Institute of Research and Innovation, Shenzhen 518057, China
* Correspondence: jinbao@hku.hk

Abstract: Tree-ring blue intensity (BI) has been widely applied for temperature reconstructions in many regions around the globe. However, it remains untested in the southeastern Tibetan Plateau (TP) where a large number of ancient trees are distributed. In this study, we developed earlywood blue intensity (EWBI), latewood blue intensity (LWBI), and delta blue intensity (ΔBI) chronologies based on tree-ring samples collected from *Abies spectabilis* at two sites in the southeastern TP. Our results reveal that the EWBI and ΔBI chronologies correlated negatively with temperature parameters and LWBI chronology correlated positively with temperature parameters, respectively. Among them, the LWBI chronology was identified most suitable for reconstructing the mean temperature in August. A linear regression model was developed for the August temperature reconstruction, which accounts for 34.31% of the observed variance in the period of 1954–2017. The reconstruction, spanning 1789–2017, is highly consistent with other tree-rings based temperature reconstructions from the neighboring regions. Our findings reveal a potential linkage between the August temperature anomaly in the southeastern TP and the Atlantic Multidecadal Oscillation (AMO), which suggests that the AMO fingerprint in the region is not just evident in winter but also in summer.

Keywords: tree-ring; blue intensity; august temperature; southeastern Tibetan Plateau; Atlantic Multidecadal Oscillation

Citation: Li, T.; Li, J. August Temperature Reconstruction Based on Tree-Ring Latewood Blue Intensity in the Southeastern Tibetan Plateau. *Forests* **2023**, *14*, 1441. https://doi.org/10.3390/f14071441

Academic Editor: Jianguo Huang

Received: 15 June 2023
Revised: 29 June 2023
Accepted: 11 July 2023
Published: 13 July 2023

1. Introduction

The Tibetan Plateau (TP), known as the "third pole" [1], plays a vital role in regulating atmospheric circulations in both East Asia and South Asia due to its substantial thermal and mechanical impacts [2,3]. Instrumental climate data have presented a rapid warming on the TP over the past six decades that surpasses the global average warming rate [4,5]. This remarkable warming has contributed, to a certain extent, to the accelerated glacier melting [6] and land degradation in the region [7]. Nevertheless, our understanding of temperature change on the TP remains limited because of the scarcity of long-term, high-resolution climate records.

Tree-rings have played a key role in paleoclimate reconstructions spanning the past centuries to millennia, owing to their precise dating, annual resolution, and extensive geographical distribution [8–10]. In recent years, there have been many tree-ring based temperature reconstructions focusing on the TP owing to the dramatic temperature increase in the region [11–16]. However, most of the tree-ring based temperature reconstructions are developed from relatively high-elevation regions on the TP. This is because tree-ring formation is primarily controlled by temperature at high-elevation sites, whereas by precipitation or a combination of temperature and precipitation at low-elevation sites [17]. As a result, fewer tree-ring based temperature reconstructions have been conducted for the relatively low-elevation regions on the TP, especially for summer temperature.

Numerous studies have attempted to maximize the temperature signals derived from tree-rings by utilizing various types of parameters. It has been established that tree-ring density generally exhibits higher sensitivity to temperature compared to other tree-ring parameters [18,19]. Accordingly, the maximum latewood density (MXD) of tree-rings has been employed for the summer temperature reconstructions [16,20]. Nonetheless, the X-ray method, which is the testing method of tree-ring density, has disadvantages such as the cumbersome and lengthy measurement process [21], which leads to relatively less work based on tree-ring density.

McCarroll et al. (2002) introduced a swift and easily accessible method for obtaining microdensitometric data utilizing reflected light rather than X-ray radiation. This innovative technique allows for the quantification of lignin concentration, commonly identified as blue intensity (BI) [22]. In the past two decades, the BI technology has been widely applied in climate reconstructions in Europe [23–25], North America [26,27], and Australia [28]. Among them, latewood blue intensity (LWBI) has shown the capability to replace MXD in the reconstruction of summer temperature [29–31]. Up to date, the BI-based tree-ring studies have rarely been carried out in China. Among the first attempts, Cao et al. (2022) found for the first time that the earlywood blue intensity (EWBI) and latewood blue intensity (LWBI) in southeast China have distinct climate signals [32], which have been further explored for temperature reconstruction [33]. Nonetheless, previous BI studies were mostly carried out in high or low altitude areas, and its effectiveness in the low-elevation regions of the TP remains unknown. Therefore, this study aims to establish the first BI-based chronologies using tree-rings collected from two sites of *Abies spectabilis* on the southeastern TP. The BI chronologies will be assessed for their sensitivity to climate factors as well as the potential for climate reconstruction.

2. Materials and Methods

2.1. Study Area

Our two sampling sites are located in the central part of the Hengduan Mountains on the southeastern TP (Figure 1, Table 1), with elevations ranging from 4100 m to 4200 m above sea level (a.s.l). The study area is jointly influenced by the East Asian monsoon and the South Asian monsoon, with precipitation mainly concentrated in May to August. Based on observations from the nearest meteorological station (Deqin, 28.48° N, 98.92° E, 3319 m a.s.l) during the period 1954–2017, the highest temperature and precipitation are both found in July, with an average value of 12.7 °C and 133 mm, respectively (Figure 2a). The temperature has shown a remarkable increasing trend over the past 60 years (Figure 2b), while precipitation and the self-calibrating Palmer Drought Severity Index [34,35] have displayed a weak decreasing trend (Figure 2c,d).

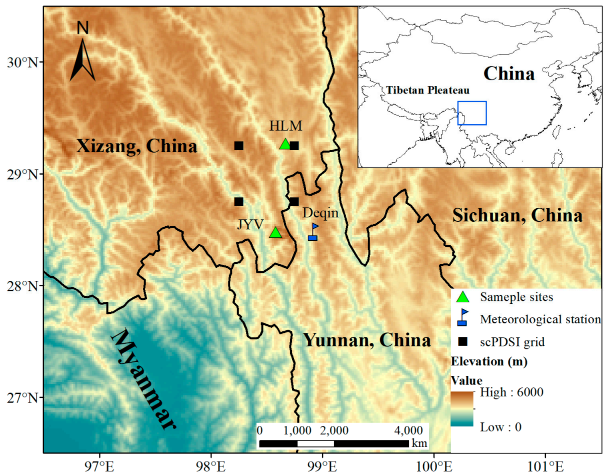

Figure 1. Map of the southeastern TP showing the location of the tree-ring sampling sites, the Deqin meteorological station, and the four scPDSI grid points.

Table 1. Location of the tree sites and the nearest meteorological station.

Site	Latitude	Longitude	Elevation (m)	Species	Cores/Trees
HLM	29.27° N	98.67° E	4160	*Abies spectabilis*	64/30
JYV	28.48° N	98.58° E	4200	*Abies spectabilis*	52/26
Deqin	28.48° N	98.92° E	3319		

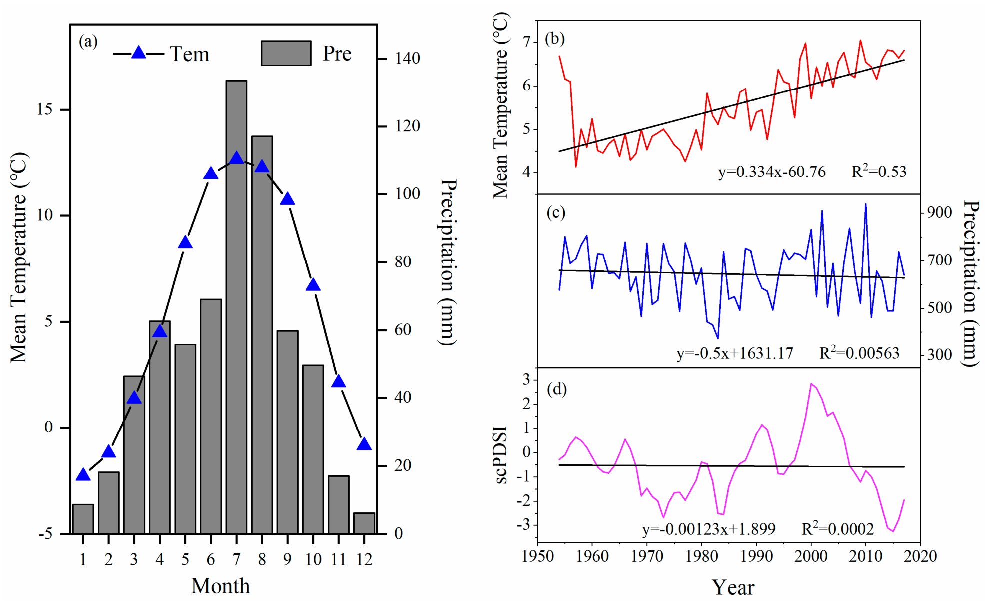

Figure 2. (**a**) Monthly distribution of mean temperature and total precipitation based on climate data from Deqin meteorological station. Temporal variability of (**b**) annual mean temperature, (**c**) annual total precipitation, and (**d**) annual mean scPDSI during the period 1954–2017.

2.2. Tree-Ring Data

We collected tree-ring samples from living *A. spectabilis* trees in the Hongla Mountain (HLM) and Jiaying Village (JYV) sites on the southeastern TP (Figure 1). A total of 116 cores from 56 trees were retrieved from the two sites, with at least two cores taken from each tree at a height of 1.3 m above the ground. The tree core samples were brought back to the lab, air-dried, mounted, and polished following the standard methods of dendrochronology [36]. As there exists a visible color difference between heartwood and sapwood of *A. spectabilis*, the tree cores were pre-treated with resin extraction. Tree core samples were refluxed in solvents of ethanol in a water bath (120 °C) for approximately 48 h [32]. The samples were sanded using sandpapers from 300 grit, to 600 grit, to 1200 grit. This process ensures a smooth and flat surface on the core samples, thereby enhancing the quality of the scanned images [37]. The samples were scanned with a flatbed scanner (Epson PerfectionV800 photo) that was calibrated with SilverFast Ai Studio (Version 8.8) software. The color was calibrated with Kodak (Advanced Color Calibration Target IT8.7/2). The samples were subsequently scanned at 4800 dpi resolution. To minimize any potential distortions caused by ambient light, a specially designed box with a black-lined inner surface was employed during the scanning procedure [38]. For the measurement of tree-ring width (TRW), earlywood blue intensity (EWBI), and latewood blue intensity (LWBI), we utilized the image analysis software CooRecorder 9.3 [39]. To distinguish the boundaries between earlywood and latewood within annual rings (Figure 3), we relied on the distinct color transition resulting from the variations in tracheid cell size and cell wall thickness. The tree-ring series were rigorously cross-dated through visual comparison of their growth patterns and statistically validated using the program COFECHA [40]. Ultimately, a subset of 108 cores with robust inter-series correlation and long timespan were selected for the extraction of EWBI and LWBI (Figure 3).

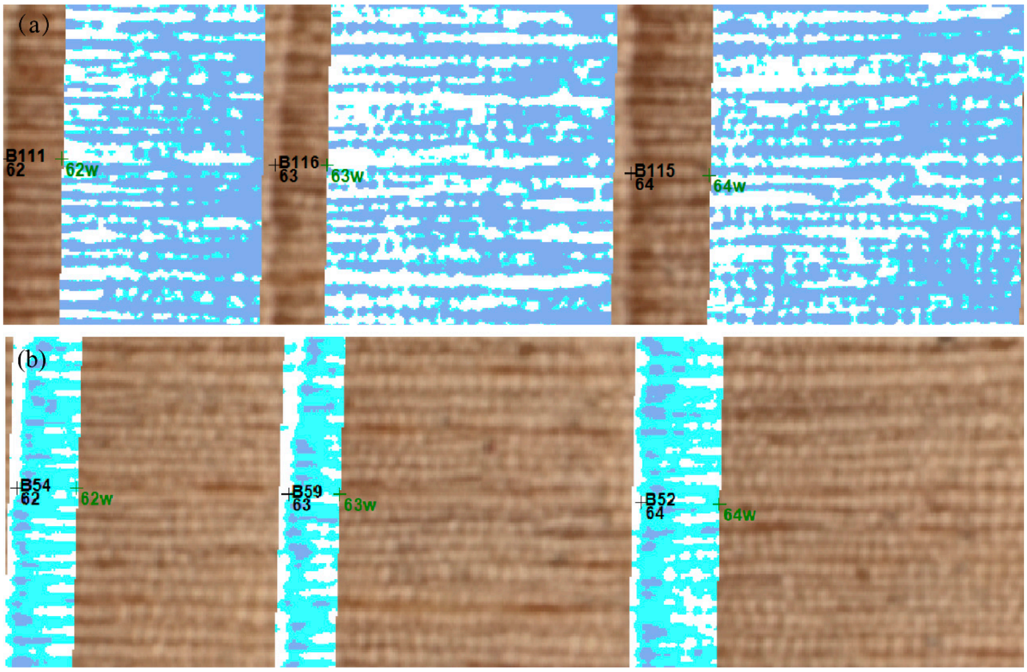

Figure 3. The measurement process of (**a**) earlywood blue intensity (EWBI) and (**b**) latewood blue intensity (LWBI) of *A. spectabilis*. The black "+" denotes the growth ring boundary and the green "+" denotes the earlywood and latewood boundary. The number on the lower right of "+" denotes the annual ring number; the year value denotes the age; the number after "B" indicates the BI value of the measured area.

In order to achieve color data, we employed the "mean of sorted pixels" approach, specifically calculating the mean of the 15 percent darkest pixels for the latewood parameter and the mean of the 80 percent lightest pixels for the earlywood parameter [38]. With an increase in the density of tree-rings, the absorption of BI intensifies, leading to a decrease in the reflectance of BI at the surface of the tested sample cores. Consequently, we observed a negative correlation between BI and tree-ring density [41]. To streamline further analysis, we utilized formula (1) for the purpose of conversion:

$$BI_{(adj)} = 2.56 - BI/100 \tag{1}$$

In the formula, BI represents the original value of blue intensity for a specific year. The constant 2.56 is employed to ensure that $BI_{(adj)}$ does not fall below 0, considering that all BI values range between 0 and 255. It is worth noting that this conversion step is optional and serves as an output feature of CooRecorder 9.3 [38]. After the conversion, the tree-ring BI exhibits a positive correlation with its density.

In addition, the EWBI records were taken away from the LWBI records to generate the delta blue intensity (ΔBI) data [41]. To remove age-related growth trend, the tree-ring series were detrended conservatively by fitting a negative exponential curve or linear line of any slope using the ARSTAN program [42]. The standard chronology was developed by averaging the individual sequences with the bi-weight robust mean method for each tree-ring parameter (Figure 4). The reliable portion of each chronology was determined using the subsample signal strength (SSS) value of 0.85 [43]. Statistics of TRW, EWBI, LWBI, and ΔBI chronologies are shown in Table 2.

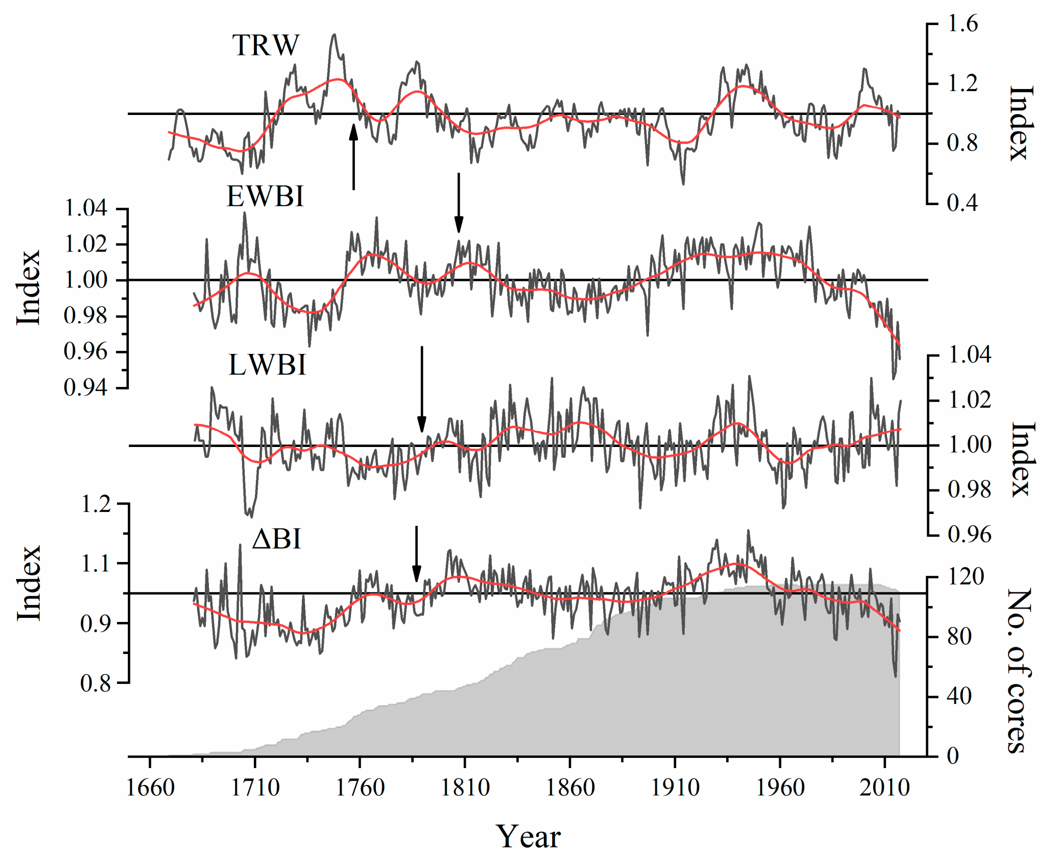

Figure 4. The TRW, EWBI, LWBI, and ΔBI chronologies developed in this study. The gray shaded area at the bottom denotes tree cores numbers through time. The arrow indicates the starting year with SSS value over 0.85. Red bold curve denotes 10-year low-pass filter of each series. The black straight line denotes the mean of each chronology.

Table 2. Statistics of the four types of tree-ring chronologies used in this study.

Statistic	TRW	EWBI	LWBI	ΔBI
Mean sensitivity (MS)	0.180	0.026	0.024	0.028
Standard deviation (SD)	0.194	0.111	0.167	0.041
First-order autocorrelation (AC1)	0.848	0.828	0.742	0.555
Correlation for all cores (r1)	0.359	0.142	0.240	0.135
Correlation between trees (r2)	0.131	0.129	0.170	0.138
Correlation within trees (r3)	0.189	0.109	0.165	0.134
Signal-to-noise ratio (SNR)	11.891	4.447	6.363	6.949
Expressed population signal (EPS)	0.922	0.816	0.864	0.874
First year SSS > 0.85	1757	1807	1789	1783

2.3. Climate Data

Monthly temperature and precipitation records from the Deqin meteorological station during the period 1954–2017 were obtained from the China Meteorological Data Network (http://data.cma.cn/, accessed on 1 June 2021). Furthermore, the Climatic Research Unit (CRU) temperature and self-calibrating Palmer Drought Index (scPDSI) datasets, available at a spatial resolution of 0.5° × 0.5°, were utilized [34,35]. The scPDSI is derived from observed precipitation and temperature-driven water balance model and calibrated to local climate conditions. We acquired four gridded scPDSI data nearest to the two sampling sites (Figure 1, Table 1). These data were averaged to generate a time series reflecting drought conditions in the study area. To investigate the potential impact of large-scale ocean-atmospheric circulation on regional climate, we examined the linkage of tree-rings to the Atlantic Multidecadal Oscillation (AMO) using the instrumental data [44].

2.4. Statistical Methods

In order to assess the climate–growth relationships, we calculated the Pearson's correlations between TRW, EWBI, LWBI, and ΔBI chronologies and monthly temperature, precipitation, scPDSI from previous November to current September. The first-order differences of each chronology and climate factors were also calculated to eliminate the impact of the long-term trend on the climate–tree growth relationship. The climate variable that exhibited the highest correlation with the tree-ring chronology was chosen for reconstruction with a linear regression model [45]. The reliability of the reconstruction model was assessed through a split-sample calibration and verification approach [46], employing statistical parameters such as the reduction of error (RE), coefficient of efficiency (CE), and the sign test (ST). In addition, the multi-taper method (MTM) spectral analysis was conducted in order to identify the periodic variations of the reconstructed series [47].

3. Results

The reliable portion of the TRW, EWBI, LWBI, and ΔBI chronologies spans the past 261 (1757–2017), 211 (1807–2017), 229 (1789–2017), and 234 (1787–2017) years, respectively (Figure 4). Significant correlations ($p < 0.01$) of TRW chronology with temperature are found in current April (r = 0.38) and August (r = 0.34) (Figure 5a). However, the first difference of TRW chronology only exhibits significant negative correlation ($r = -0.28$, $p < 0.05$) with June temperature (Figure 6a). Significant negative correlations of EWBI chronology with temperature are found in all months investigated, but all the correlations become non-significant for the first-difference series (Figures 5b and 6b). Significant negative correlation is also found between ΔBI chronology and temperature in current June ($r = -0.51$; $p < 0.01$), yet the correlation becomes non-significant for the first-difference series (Figures 5d and 6d). In contrast, the positive correlations of LWBI chronology with temperature are significant for both raw and first-difference series in current July to September (Figures 5c and 6c), suggesting that the LWBI chronology contains the strongest and most reliable temperature signals among the four types of the chronologies.

All the four chronologies exhibit generally weak correlations with precipitation, despite the marginally significant correlations ($p < 0.05$) that are found with TRW chronology in current May, EWBI and ΔBI chronologies in current June, and LWBI chronology in current August. These results suggest that precipitation has rather weak influence on tree growth at our sampling sites. On the other hand, both TRW and EWBI chronologies show significant positive correlations with the scPDSI in several months, suggesting that they might be good parameters to reflect moisture condition at the sampling sites. Nonetheless, the highest correlation is found between LWBI chronology and August temperature (r = 0.59), and the correlation between their first-difference series is still significant (r = 0.44) (Figures 5c and 6c).

Considering that the highest correlation is found between LWBI chronology and August temperature, a linear regression model was developed between them for reconstruction (Figure 7a). The reconstruction accounts for 34.31% of the variance during the common period of 1954 to 2017 and exhibits good agreements with the observed August temperature at both high-frequency and low-frequency bands (Figure 7b). The RE and CE values are both positive, demonstrating the reliability of the reconstruction model (Table 3). The ST values are all significant above the 99.9% confidence level, further validating the accuracy of the reconstruction. We reconstructed the temporal changes in August temperature from 1789 to 2017 based on this model (Figure 7c). Based on the threshold value of two standard deviations from the mean (mean $\pm$ 2σ), we identified nine extremely warm (1831, 1851, 1866, 1937, 1945, 2003) and four extremely cold (1817, 1893, 1961, 1962) years in the reconstruction. Based on the 10-year low-pass filter of the reconstruction series, five extremely warm (1799–1807, 1822–1842, 1848–1875, 1927–1950, 2002–2010) and four extremely cold

(1789–1798, 1808–1821, 1887–1926, 1954–1976) epochs, defined as at least nine persistently warm/cold years, were further identified in the reconstruction. Spatial correlations of the observed and reconstructed August temperature with the gridded CRU temperature data show that our reconstruction can represent large-scale temperature change on the southeastern TP (Figure 8). Comparisons of our reconstruction in this study with other independent tree-ring-based temperature series from neighboring regions showed good agreement in the relatively warm and cold intervals, despite that our reconstruction is more similar to the tree-ring density reconstruction than the tree-ring width reconstructions (Figure 9). The MTM spectral analysis revealed that the temperature reconstruction exhibits several significant cycles at 2–4 years and 68–73 years (Figure 10).

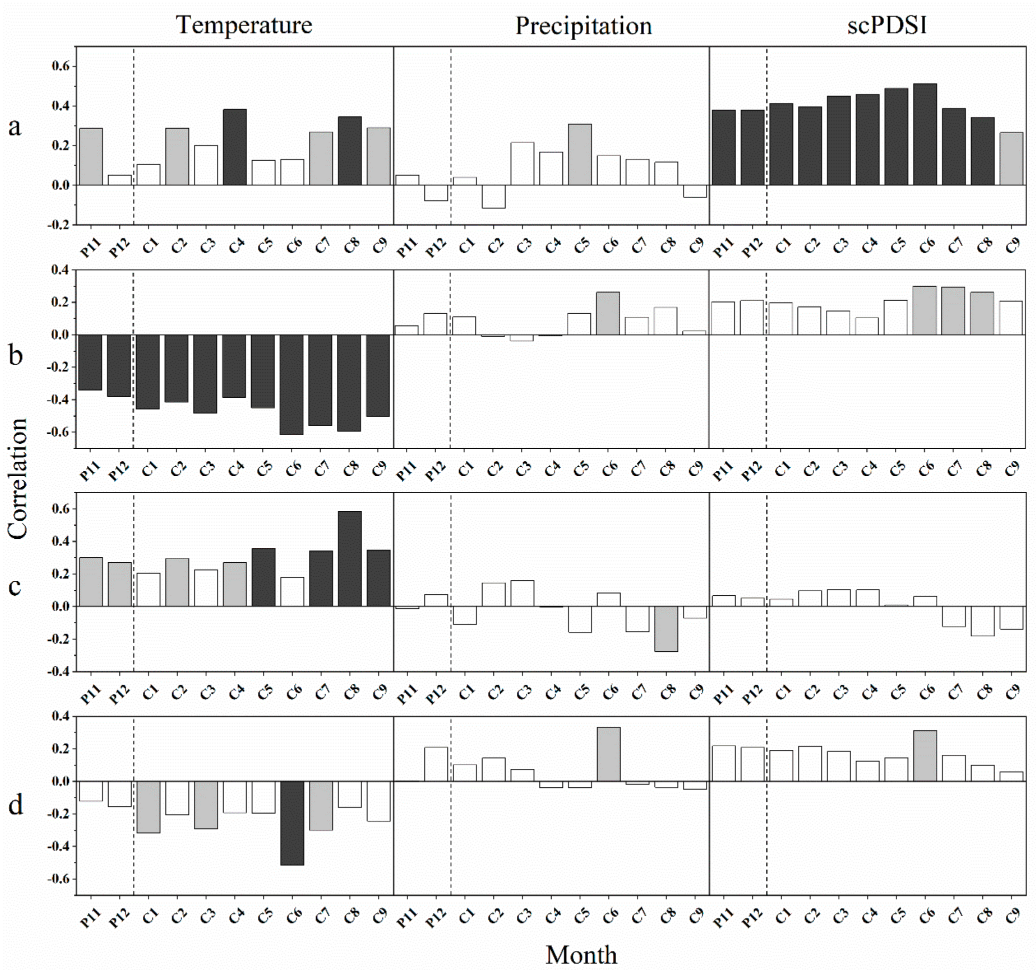

Figure 5. The Pearson's correlations of (**a**) TRW, (**b**) EWBI, (**c**) LWBI, and (**d**) ΔBI chronology with monthly temperature (**left**), precipitation (**center**), and the scPDSI (**right**) during the period 1954–2017. The gray and black shadings denote the 0.05 and 0.01 significance level, respectively.

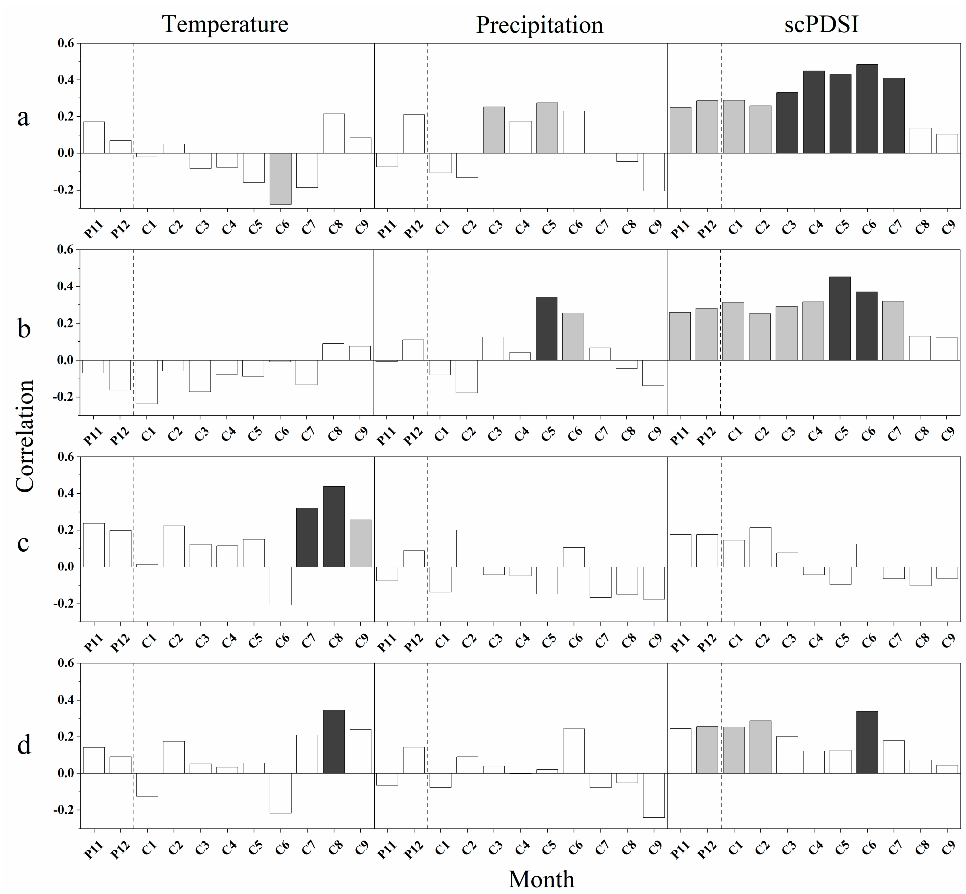

Figure 6. Same as in Figure 5, but for the first difference of the (**a**) TRW, (**b**) EWBI, (**c**) LWBI, and (**d**) ΔBI chronology.

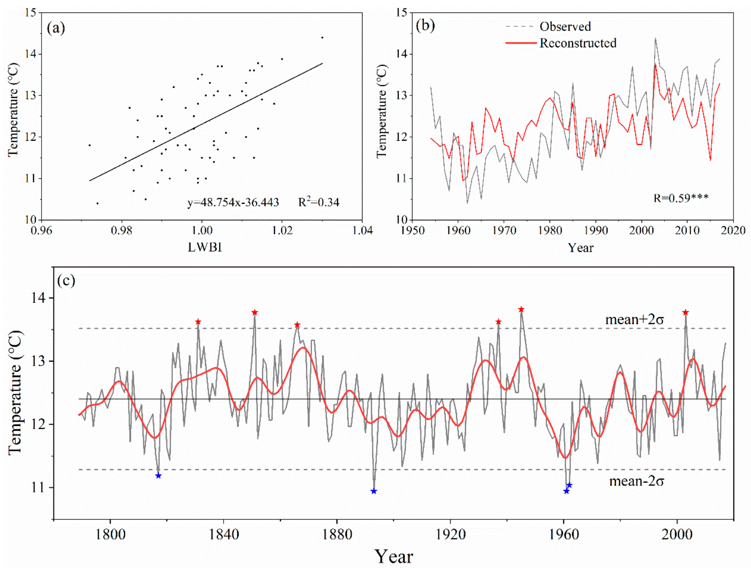

Figure 7. (**a**) Scatter plot between the LWBI chronology and August mean temperature from 1954 to 2017; (**b**) Comparison between the actual and reconstructed temperature from 1954 to 2017; (**c**) Reconstructed August mean temperature on the southeastern TP during the period 1789–2017 (grey) and its 10-year low-pass filter (red). Horizontal dashed line denotes two standard deviations away from the mean. The red/blue star indicates the extremely warm/cold years in the reconstruction. *** denotes the 0.001 significance level.

Table 3. Calibration and verification statistics of the reconstruction.

	Calibration (1954–1985)	Verification (1986–2017)	Calibration (1986–2017)	Verification (1954–1985)	Full Calibration (1954–2017)
R	0.414	0.641	0.641	0.414	0.586
R^2	0.172	0.410	0.410	0.172	0.343
CE	-	0.410	-	0.172	-
RE	-	0.821	-	0.761	-
Sign test	19+/13− ***	28+/4− ***	21+/11− ***	27+/5− ***	22+/42− ***

*** $p < 0.001$.

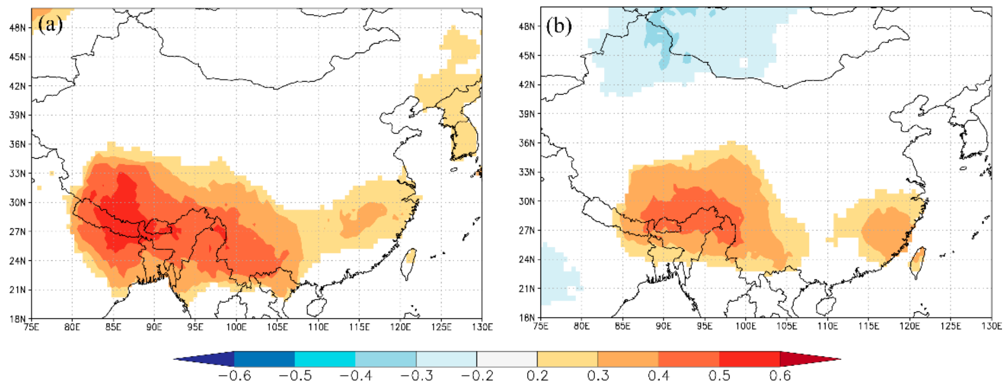

Figure 8. Spatial correlations of (**a**) actual and (**b**) reconstructed August temperature with regional gridded temperature for the period of 1954–2017.

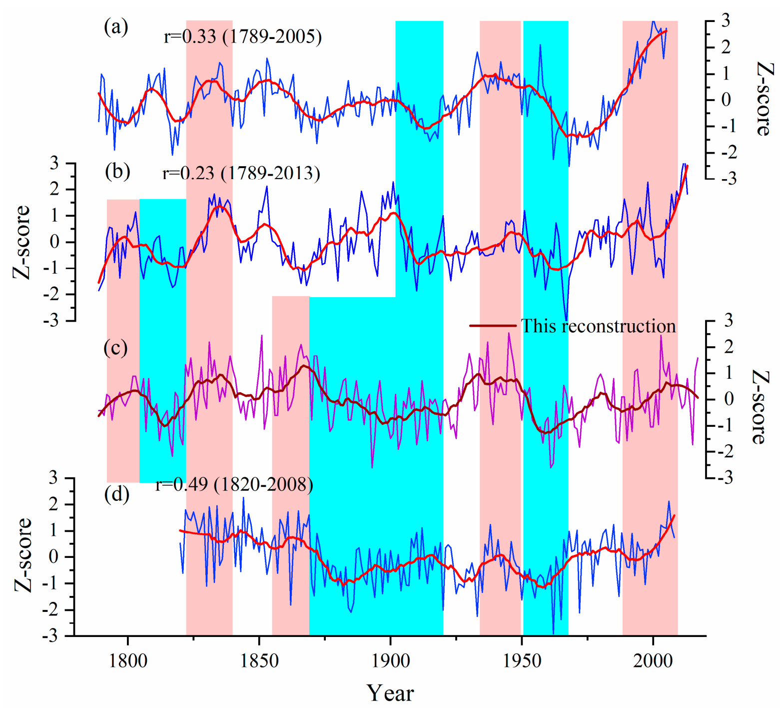

Figure 9. Comparison of the August temperature reconstruction with three tree-ring based temperature reconstructions in the nearby regions. (**a**) The annual mean temperature reconstruction on the southeastern TP [12], (**b**) the summer mean temperature reconstruction in the Bhutanese Himalaya [48], (**c**) the August mean temperature reconstruction from this study, and (**d**) late summer temperature reconstruction in Sygera Mountain, southeastern TP [49]. Reconstructions in (**a**,**b**) are based on tree-ring width, whereas reconstruction in (**d**) is based on tree-ring density. The blue and red shadings denote the common cold and warm periods, respectively.

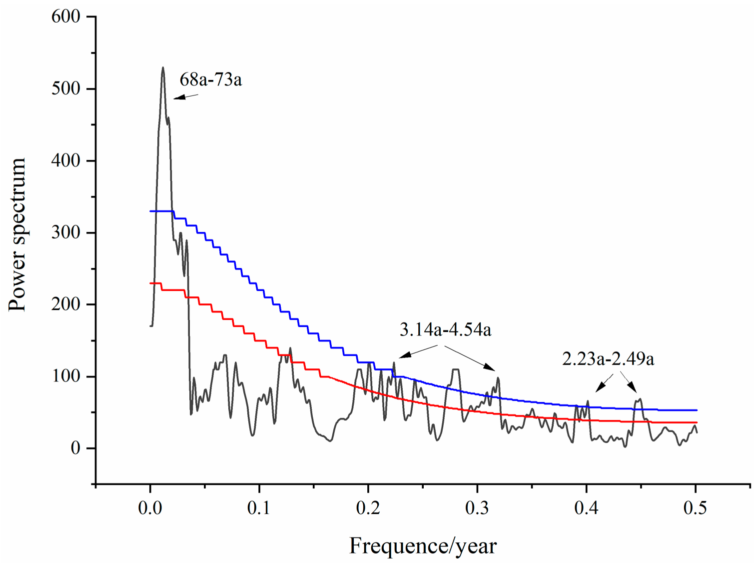

Figure 10. The MTM spectral results of the August temperature reconstruction. The red and blue curves denote the 0.05 and 0.01 significance level, respectively.

4. Discussion

4.1. Climate–Growth Relationships

The TRW and EWBI chronologies exhibit high correlations with the scPDSI (Figures 5 and 6), probably reflecting the impacts of drought conditions on tree growth during the early stage of the growing season at the sampling sites. Prior to the arrival of the monsoon rainfall, severe drought conditions can delay the lignification process in conifer trees, and even disrupt or temporarily halt tree cambium activity [50,51]. Consequently, trees are prone to forming narrow or even absent rings during drought events, resulting in low earlywood density [52]. In contrast, the LWBI chronology exhibits high correlations with temperature in summer. With abundant precipitation in summer, high summer temperature leads to the formation of larger cells and increased deposition of cell wall materials. As a result, there will be a large increase in the latewood density in such years [41,53,54]. Additionally, high summer temperature promotes an extended growing season, facilitating greater lignification in trees and the accumulation of additional lignin [55]. Both factors contribute to an increase in LWBI values.

4.2. Two Centuries of August Temperature on the Southeastern TP

Based on the climate–growth relationships, the temporal changes in August temperature on the southeastern TP was reconstructed from 1789 to 2017 (Figure 7c). Spatial correlation analysis reveals that our reconstruction can represent large-scale temperature change on the southeastern TP (Figure 8). To further validate our reconstruction and assess its large-scale representativeness, we compared the reconstruction with three temperature reconstructions from nearby regions, including an annual mean temperature reconstruction on the southeastern TP, a summer mean temperature reconstruction in the Bhutanese Himalaya, and a late summer temperature reconstruction in the Sygera Mountain on the southeastern TP [12,48,49]. These reconstructions show highly consistent warm and cold variations over their common periods, such as in 1808–1821, 1927–1950, 1951–1976, 2002–2010 (Figure 9). The extremely cold event in 1817 may be associated with the cooling effect caused by the eruption of Mount Tambora in 1815. This cooling event is widely documented in tree-ring records on the southeastern TP [56]. Our reconstruction shows that the longest warm epoch was from 1848 to 1875, which was also found in the temperature reconstructions in Chamdo County [18,57] and the Gaoligong Mountain [11,16] on the southeastern TP. Historical documents indicated an abnormally cold climate in Lhasa and Tibet during the early 1900s [58], which aligns with the cold period in our temperature reconstruction from 1886 to 1927. Furthermore, the rapid warming since the 1960s in our reconstruction was also evident in other temperature series (Figure 9). Nonetheless, our reconstruction exhibits higher similarity to the tree-ring density reconstruction [49] than the tree-ring width reconstructions [12,48]. Notably, both our reconstruction and the tree-ring density reconstruction indicated a cooling trend from the 1870s to the 1890s, whereas the tree-ring width reconstructions suggest a warming trend (Figure 9). This divergence could be attributed to the amplified seasonal temperature differences over this period [59], wherein the reconstructions based on LWBI and MXD predominantly reflect the summer temperature, whereas the tree-ring width based reconstructions reflect winter or year-round temperature.

4.3. Linkage of August Temperature with the AMO

The Atlantic Multidecadal Oscillation (AMO) denotes the oscillatory rhythm between periods of heightened and subdued states in the North Atlantic sea surface temperatures (SSTs), manifesting at approximate intervals of 60 to 80 years [60–63]. This phenomenon has played a crucial role in modulating the temperature fluctuations in the Northern Hemisphere during the 20th century [62]. The warm/cold periods of AMO are generally consistent with the positive/negative temperature anomalies across Europe [64] and East Asia [63]. The notable cycle of 68–73 years in our temperature reconstruction corresponds to the oscillation period observed in the SST variations in the North Atlantic [60–63]. Spatial correlation analysis also reveals strong positive correlations between August temperature on the southeastern TP and the SSTs in the North Atlantic (Figure 11). Moreover, our reconstruction demonstrates a significant positive correlation (r = 0.53, $p < 0.001$) with the observed AMO index during the period 1870–2017 (Figure 12). Together, these results support the notion that multidecadal temperature variations on the southeastern TP may be modulated by the AMO, with warm temperatures occurring during the positive phase of the AMO. Nonetheless, previous studies generally indicated the potential linkage of the AMO with winter temperature on the southeastern TP [12,13,63,65]. Our results indicate that the AMO influence on temperature on the southeastern TP is evident not only in winter but also in summer.

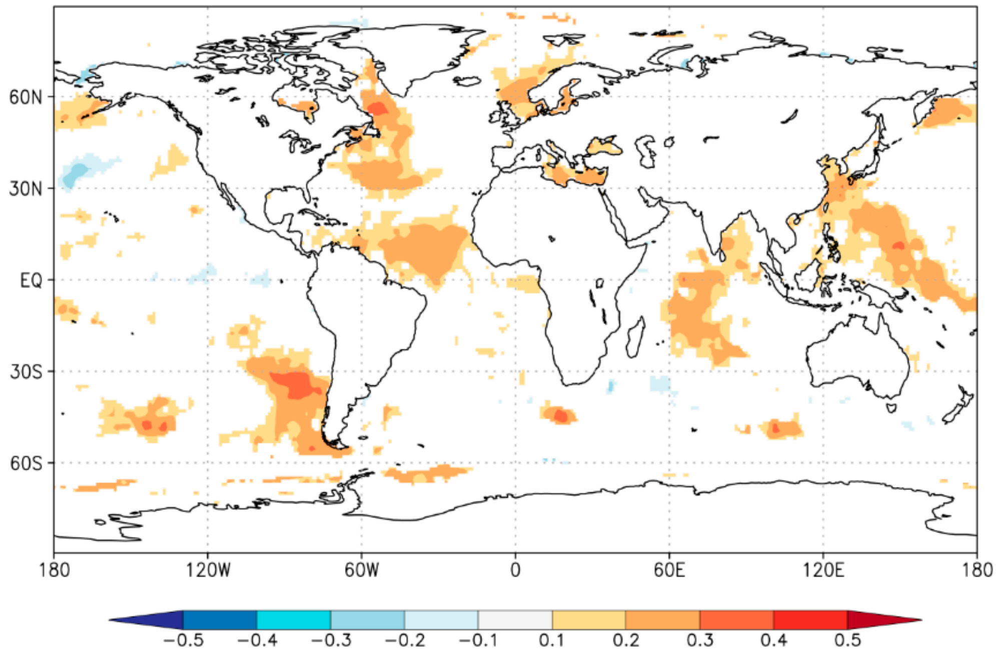

Figure 11. Spatial correlations of the temperature reconstruction with global SSTs in August for the period of 1870 to 2017.

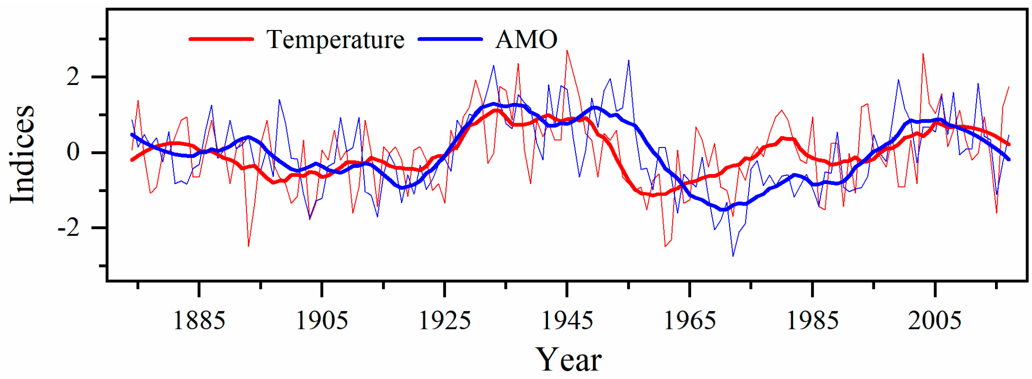

Figure 12. Comparison of the temperature reconstruction with the observed AMO index during the period 1870–2017. Bold curve denotes 10-year low-pass filter of each series. All series are standardized over their common period for direct comparison.

5. Conclusions

This study utilized the BI technique to extract density-related information from *A. spectabilis* trees in the southeastern TP. Our results indicate that the TRW and EWBI parameters exhibit high sensitivity to drought conditions, whereas the LWBI parameter is more sensitive to summer temperature. Therefore, LWBI is a potential parameter that can be used for summer temperature reconstructions on the southeastern TP. Using this approach, we reconstructed the August temperature variability over a period of 229 years on the southeastern TP. The reconstruction reveals several major warm and cold periods that are highly consistent with previous ring-width or maximum density-based temperature reconstructions in the region. Our results also reveal a potential linkage of the temperature reconstruction with the AMO, suggesting that the AMO affects not only winter but also summer temperatures over the past centuries on the southeastern TP.

Author Contributions: J.L. conceptualized the study. T.L. and J.L. conducted the field investigation. T.L. wrote the original draft, with contributions from J.L. for review and editing. All authors have read and agreed to the published version of the manuscript.

Funding: This research was funded by the National Key Research and Development Program of China (No. 2018YFA0605601), Hong Kong Research Grants Council (No. 106220169) and the National Natural Science Foundation of China (No. 42105155).

Data Availability Statement: The data presented in this study are available on request from the corresponding author.

Conflicts of Interest: The authors declare no conflict of interest. The funders had no role in the design of the study; in the collection, analyses, or interpretation of data; in the writing of the manuscript; or in the decision to publish the results.

References

1. Yao, T.; Thompson, L.G.; Mosbrugger, V.; Zhang, F.; Ma, Y.; Luo, T.; Xu, B.; Yang, X.; Joswiak, D.R.; Wang, W. Third pole environment (TPE). *Environ. Dev.* **2012**, *3*, 52–64. [CrossRef]
2. Webster, P.J.; Magana, V.O.; Palmer, T.N.; Shukla, J.; Tomas, R.A.; Yanai, M.U.; Yasunari, T. Monsoons: Processes, predictability, and the prospects for prediction. *J. Geophys. Res. Ocean.* **1998**, *103*, 14451–14510. [CrossRef]
3. Ding, Y. Effects of the Qinghai-Xizang (Tibetan) plateau on the circulation features over the plateau and its surrounding areas. *Adv. Atmos. Sci.* **1992**, *9*, 112–130.
4. Mountain Research Initiative EDW Working Group. Elevation-dependent warming in mountain regions of the world. *Nat. Clim. Chang.* **2015**, *5*, 424–430. [CrossRef]
5. You, Q.; Jiang, Z.; Moore, G.W.K.; Bao, Y.; Kong, L.; Kang, S. Revisiting the relationship between observed warming and surface pressure in the Tibetan Plateau. *J. Clim.* **2017**, *30*, 1721–1737. [CrossRef]
6. Yao, T.; Wang, Y.; Liu, S.; Pu, J.; Shen, Y.; Lu, A. Recent glacial retreat in High Asia in China and its impact on water resource in Northwest China. *Sci. China Ser. D Earth Sci.* **2004**, *47*, 1065–1075. [CrossRef]
7. Cyranoski, D. Climate change: The long-range forecast. *Nature* **2005**, *438*, 275–277. [CrossRef] [PubMed]

8. Yang, B.; Qin, C.; Wang, J.; He, M.; Melvin, T.M.; Osborn, T.J.; Briffa, K.R. A 3500-year tree-ring record of annual precipitation on the northeastern Tibetan Plateau. *Proc. Natl. Acad. Sci. USA* **2014**, *111*, 2903–2908. [CrossRef]
9. Zhang, Q.-B.; Fang, O. Tree rings circle an abrupt shift in climate. *Science* **2020**, *370*, 1037–1038. [CrossRef]
10. Cook, E.R.; Anchukaitis, K.J.; Buckley, B.M.; D'Arrigo, R.D.; Jacoby, G.C.; Wright, W.E. Asian monsoon failure and megadrought during the last millennium. *Science* **2010**, *328*, 486–489. [CrossRef]
11. Fan, Z.-X.; Bräuning, A.; Tian, Q.-H.; Yang, B.; Cao, K.-F. Tree ring recorded May–August temperature variations since AD 1585 in the Gaoligong Mountains, southeastern Tibetan Plateau. *Palaeogeogr. Palaeoclimatol. Palaeoecol.* **2010**, *296*, 94–102. [CrossRef]
12. Wang, J.; Yang, B.; Qin, C.; Kang, S.; He, M.; Wang, Z. Tree-ring inferred annual mean temperature variations on the southeastern Tibetan Plateau during the last millennium and their relationships with the Atlantic Multidecadal Oscillation. *Clim. Dyn.* **2014**, *43*, 627–640. [CrossRef]
13. Shi, S.; Li, J.; Shi, J.; Zhao, Y.; Huang, G. Three centuries of winter temperature change on the southeastern Tibetan Plateau and its relationship with the Atlantic Multidecadal Oscillation. *Clim. Dyn.* **2017**, *49*, 1305–1319. [CrossRef]
14. Liang, E.Y.; Shao, X.M.; Xu, Y. Tree-ring evidence of recent abnormal warming on the southeast Tibetan Plateau. *Theor. Appl. Climatol.* **2009**, *98*, 9–18. [CrossRef]
15. Liang, H.; Lyu, L.; Wahab, M. A 382-year reconstruction of August mean minimum temperature from tree-ring maximum latewood density on the southeastern Tibetan Plateau, China. *Dendrochronologia* **2016**, *37*, 1–8. [CrossRef]
16. Li, M.-Y.; Wang, L.; Fan, Z.-X.; Shen, C.-C. Tree-ring density inferred late summer temperature variability over the past three centuries in the Gaoligong Mountains, southeastern Tibetan Plateau. *Palaeogeogr. Palaeoclimatol. Palaeoecol.* **2015**, *422*, 57–64. [CrossRef]
17. He, M.; Yang, B.; Bräuning, A.; Rossi, S.; Ljungqvist, F.C.; Shishov, V.; Grießinger, J.; Wang, J.; Liu, J.; Qin, C. Recent advances in dendroclimatology in China. *Earth-Sci. Rev.* **2019**, *194*, 521–535. [CrossRef]
18. Wang, L.; Duan, J.; Chen, J.; Huang, L.; Shao, X. Temperature reconstruction from tree-ring maximum density of Balfour spruce in eastern Tibet, China. *Int. J. Climatol.* **2010**, *30*, 972–979. [CrossRef]
19. Duan, J.; Zhang, Q.-B. A 449 year warm season temperature reconstruction in the southeastern Tibetan Plateau and its relation to solar activity. *J. Geophys. Res. Atmos.* **2014**, *119*, 11–578. [CrossRef]
20. Xing, P.; Zhang, Q.-B.; Lv, L.-X. Absence of late-summer warming trend over the past two and half centuries on the eastern Tibetan Plateau. *Glob. Planet. Chang.* **2014**, *123*, 27–35. [CrossRef]
21. Schweingruber, F.H.; Fritts, H.C.; Bräker, O.U.; Drew, L.G.; Schär, E. The X-ray technique as applied to dendroclimatology. *Tree-Ring Bull.* **1978**, *38*, 61–91.
22. McCarroll, D.; Pettigrew, E.; Luckman, A.; Guibal, F.; Edouard, J.L. Blue reflectance provides a surrogate for latewood density of high-latitude pine tree rings. *Arct. Antarct. Alp. Res.* **2002**, *34*, 450–453. [CrossRef]
23. Fuentes, M.; Salo, R.; Björklund, J.; Seftigen, K.; Zhang, P.; Gunnarson, B.; Aravena, J.-C.; Linderholm, H.W. A 970-year-long summer temperature reconstruction from Rogen, west-central Sweden, based on blue intensity from tree rings. *Holocene* **2018**, *28*, 254–266. [CrossRef]
24. Rydval, M.; Loader, N.J.; Gunnarson, B.E.; Druckenbrod, D.L.; Linderholm, H.W.; Moreton, S.G.; Wood, C.V.; Wilson, R. Reconstructing 800 years of summer temperatures in Scotland from tree rings. *Clim. Dyn.* **2017**, *49*, 2951–2974. [CrossRef]
25. McCarroll, D.; Loader, N.J.; Jalkanen, R.; Gagen, M.H.; Grudd, H.; Gunnarson, B.E.; Kirchhefer, A.J.; Friedrich, M.; Linderholm, H.W.; Lindholm, M. A 1200-year multiproxy record of tree growth and summer temperature at the northern pine forest limit of Europe. *Holocene* **2013**, *23*, 471–484. [CrossRef]
26. Wilson, R.; Rao, R.; Rydval, M.; Wood, C.; Larsson, L.-Å.; Luckman, B.H. Blue Intensity for dendroclimatology: The BC blues: A case study from British Columbia, Canada. *Holocene* **2014**, *24*, 1428–1438. [CrossRef]
27. Heeter, K.J.; Harley, G.L.; Maxwell, J.T.; Wilson, R.J.; Abatzoglou, J.T.; Rayback, S.A.; Rochner, M.L.; Kitchens, K.A. Summer temperature variability since 1730 CE across the low-to-mid latitudes of western North America from a tree ring blue intensity network. *Quat. Sci. Rev.* **2021**, *267*, 107064. [CrossRef]
28. Brookhouse, M.; Graham, R. Application of the minimum blue-intensity technique to a Southern-Hemisphere conifer. *Tree-Ring Res.* **2016**, *72*, 103–107. [CrossRef]
29. McCarroll, D.; Tuovinen, M.; Campbell, R.; Gagen, M.; Grudd, H.; Jalkanen, R.; Loader, N.J.; Robertson, I. A critical evaluation of multi-proxy dendroclimatology in northern Finland. *J. Quat. Sci.* **2011**, *26*, 7–14. [CrossRef]
30. Österreicher, A.; Weber, G.; Leuenberger, M.; Nicolussi, K. Exploring blue intensity-comparison of blue intensity and MXD data from Alpine spruce trees. *Tree Rings Archaeol. Climatol. Ecol.* **2015**, *13*, 56–61.
31. Rydval, M.; Gunnarson, B.E.; Loader, N.J.; Cook, E.R.; Druckenbrod, D.L.; Wilson, R. Spatial reconstruction of Scottish summer temperatures from tree rings. *Int. J. Climatol.* **2017**, *37*, 1540–1556. [CrossRef]
32. Cao, X.; Fang, K.; Chen, P.; Zhang, P.; Björklund, J.; Pumijumnong, N.; Guo, Z. Microdensitometric records from humid subtropical China show distinct climate signals in earlywood and latewood. *Dendrochronologia* **2020**, *64*, 125764. [CrossRef]
33. Cao, X.; Hu, H.; Kao, P.-k.; Buckley, B.M.; Dong, Z.; Chen, X.; Zhou, F.; Fang, K. Improved spring temperature reconstruction using earlywood blue intensity in southeastern China. *Int. J. Climatol.* **2022**, *42*, 6204–6220. [CrossRef]
34. van der Schrier, G.; Barichivich, J.; Briffa, K.R.; Jones, P.D. A scPDSI-based global data set of dry and wet spells for 1901–2009. *J. Geophys. Res. Atmos.* **2013**, *118*, 4025–4048. [CrossRef]

35. Harris, I.; Jones, P.D.; Osborn, T.J.; Lister, D.H. Updated high-resolution grids of monthly climatic observations—The CRU TS3. 10 Dataset. *Int. J. Climatol.* **2014**, *34*, 623–642. [CrossRef]
36. Stokes, M.A. *An Introduction to Tree-Ring Dating*; University of Arizona Press: Tucson, AZ, USA, 1996.
37. Babst, F.; Frank, D.; Büntgen, U.; Nievergelt, D.; Esper, J. Effect of sample preparation and scanning resolution on the Blue Reflectance of Picea abies. *TRACE Proc* **2009**, *7*, 188–195.
38. Rydval, M.; Larsson, L.-Å.; McGlynn, L.; Gunnarson, B.E.; Loader, N.J.; Young, G.H.F.; Wilson, R. Blue intensity for dendroclimatology: Should we have the blues? Experiments from Scotland. *Dendrochronologia* **2014**, *32*, 191–204. [CrossRef]
39. Larsson, L. *Cdendro Package Version 7*; CooRecorder and Cdendro Programs of the CooRecorder. Cybis: Saltsjöbaden, Sweden, 2014.
40. Holmes, R.L. Computer-assisted quality control in tree-ring dating and measurement. *Tree-Ring Bull.* **1983**, *43*, 69–78.
41. Björklund, J.A.; Gunnarson, B.E.; Seftigen, K.; Esper, J.; Linderholm, H.W. Blue intensity and density from northern Fennoscandian tree rings, exploring the potential to improve summer temperature reconstructions with earlywood information. *Clim. Past* **2014**, *10*, 877–885. [CrossRef]
42. Cook, E.R.; Briffa, K.R.; Jones, P.D. Spatial regression methods in dendroclimatology: A review and comparison of two techniques. *Int. J. Climatol.* **1994**, *14*, 379–402. [CrossRef]
43. Wigley, T.M.L.; Briffa, K.R.; Jones, P.D. On the average value of correlated time series, with applications in dendroclimatology and hydrometeorology. *J. Appl. Meteorol. Climatol.* **1984**, *23*, 201–213. [CrossRef]
44. van Oldenborgh, G.J.; te Raa, L.A.; Dijkstra, H.A.; Philip, S.Y. Frequency-or amplitude-dependent effects of the Atlantic meridional overturning on the tropical Pacific Ocean. *Ocean Sci.* **2009**, *5*, 293–301. [CrossRef]
45. Robinson, W.J.; Cook, E.; Pilcher, J.R.; Eckstein, D.; Kairiukstis, L.; Shiyatov, S.; Norton, D.A. Some historical background on dendrochronology. In *Methods of Dendrochronology: Applications in the Environmental Sciences*; Springer: Dordrecht, The Netherlands, 1990; pp. 1–21.
46. Fritts, H.C. *Tree Rings and Climate*; Academic Press: New York, NY, USA, 1976.
47. Mann, M.E.; Lees, J.M. Robust estimation of background noise and signal detection in climatic time series. *Clim. Chang.* **1996**, *33*, 409–445. [CrossRef]
48. Krusic, P.J.; Cook, E.R.; Dukpa, D.; Putnam, A.E.; Rupper, S.; Schaefer, J. Six hundred thirty-eight years of summer temperature variability over the Bhutanese Himalaya. *Geophys. Res. Lett.* **2015**, *42*, 2988–2994. [CrossRef]
49. Li, M.; Duan, J.; Wang, L.; Zhu, H. Late summer temperature reconstruction based on tree-ring density for Sygera Mountain, southeastern Tibetan Plateau. *Glob. Planet. Chang.* **2018**, *163*, 10–17. [CrossRef]
50. Vieira, J.; Campelo, F.; Rossi, S.; Carvalho, A.; Freitas, H.; Nabais, C. Adjustment capacity of maritime pine cambial activity in drought-prone environments. *PLoS ONE* **2015**, *10*, e0126223. [CrossRef]
51. de Luis, M.; Novak, K.; Raventós, J.; Gričar, J.; Prislan, P.; Čufar, K. Climate factors promoting intra-annual density fluctuations in Aleppo pine (*Pinus halepensis*) from semiarid sites. *Dendrochronologia* **2011**, *29*, 163–169. [CrossRef]
52. Björklund, J.; Seftigen, K.; Schweingruber, F.; Fonti, P.; von Arx, G.; Bryukhanova, M.V.; Cuny, H.E.; Carrer, M.; Castagneri, D.; Frank, D.C. Cell size and wall dimensions drive distinct variability of earlywood and latewood density in Northern Hemisphere conifers. *New Phytol.* **2017**, *216*, 728–740. [CrossRef]
53. Campbell, R.; McCarroll, D.; Robertson, I.; Loader, N.J.; Grudd, H.; Gunnarson, B. Blue intensity in Pinus sylvestris tree rings: A manual for a new palaeoclimate proxy. *Tree-Ring Res.* **2011**, *67*, 127–134. [CrossRef]
54. Björklund, J.; von Arx, G.; Nievergelt, D.; Wilson, R.; Van den Bulcke, J.; Günther, B.; Loader, N.J.; Rydval, M.; Fonti, P.; Scharnweber, T. Scientific merits and analytical challenges of tree-ring densitometry. *Rev. Geophys.* **2019**, *57*, 1224–1264. [CrossRef]
55. Campbell, R.; McCarroll, D.; Loader, N.J.; Grudd, H.; Robertson, I.; Jalkanen, R. Blue intensity in Pinus sylvestris tree-rings: Developing a new palaeoclimate proxy. *Holocene* **2007**, *17*, 821–828. [CrossRef]
56. Li, M.; Huang, L.; Yin, Z.-Y.; Shao, X. Temperature reconstruction and volcanic eruption signal from tree-ring width and maximum latewood density over the past 304 years in the southeastern Tibetan Plateau. *Int. J. Biometeorol.* **2017**, *61*, 2021–2032. [CrossRef] [PubMed]
57. Bräuning, A.; Mantwill, B. Summer temperature and summer monsoon history on the Tibetan plateau during the last 400 years recorded by tree rings. *Geophys. Res. Lett.* **2004**, *31*, L24205. [CrossRef]
58. Liu, X.; Chen, B. Climatic warming in the Tibetan Plateau during recent decades. *Int. J. Climatol.* **2000**, *20*, 1729–1742. [CrossRef]
59. Duan, J.; Esper, J.; Büntgen, U.; Li, L.; Xoplaki, E.; Zhang, H.; Wang, L.; Fang, Y.; Luterbacher, J. Weakening of annual temperature cycle over the Tibetan Plateau since the 1870s. *Nat. Commun.* **2017**, *8*, 14008. [CrossRef] [PubMed]
60. Delworth, T.L.; Mann, M.E. Observed and simulated multidecadal variability in the Northern Hemisphere. *Clim. Dyn.* **2000**, *16*, 661–676. [CrossRef]
61. Kerr, R.A. A North Atlantic climate pacemaker for the centuries. *Science* **2000**, *288*, 1984–1985. [CrossRef]
62. Zhang, R.; Delworth, T.L.; Held, I.M. Can the Atlantic Ocean drive the observed multidecadal variability in Northern Hemisphere mean temperature? *Geophys. Res. Lett.* **2007**, *34*, L02709. [CrossRef]
63. Li, S.; Bates, G.T. Influence of the Atlantic multidecadal oscillation on the winter climate of East China. *Adv. Atmos. Sci.* **2007**, *24*, 126–135. [CrossRef]

64. Sutton, R.T.; Dong, B. Atlantic Ocean influence on a shift in European climate in the 1990s. *Nat. Geosci.* **2012**, *5*, 788–792. [CrossRef]
65. Wang, Y.; Li, S.; Luo, D. Seasonal response of Asian monsoonal climate to the Atlantic Multidecadal Oscillation. *J. Geophys. Res. Atmos.* **2009**, *114*, D02112. [CrossRef]